

Influence of Graphene Oxide Nanoparticles on Bond-Slip Responses between Fiber and Geopolymer Mortar

Darrakorn Intarabut^a, Piti Sukontasukkul^{a*}, Tanakorn Phoo-ngernkham^{b*}, Hexin Zhang^c, Doo-yeol Yoo^d, Suchart Limkatanyu^e, Prinya Chindaprasirt^{f,g}

^a*Construction and Building Materials Research Center, Department of Civil Engineering, Faculty of Engineering, King Mongkut's University of Technology North Bangkok, Bangkok, Thailand*

^b*Sustainable Construction Material Technology Research Unit, Department of Civil Engineering, Faculty of Engineering and Architecture, Rajamangala University of Technology Isan, Nakhon Ratchasima, Thailand*

^c*School of Engineering and the Built Environment, Edinburgh Napier University, Edinburgh, United Kingdom*

^d*Department of Architectural Engineering, Hanyang University, Seongdong-gu, Seoul, Republic of Korea,*

^e*Department of Civil Engineering, Faculty of Engineering, Prince of Songkla, Hat Yai Campus, Songkla, Thailand*

^f*Sustainable Infrastructure Research and Development Center, Department of Civil Engineering, Faculty of Engineering, Khon Kaen University, Khon Kaen, Thailand*

^g*Academy of Science, Royal Society of Thailand, Dusit, Bangkok, Thailand*

*Corresponding author, email: piti.s@eng.kmutnb.ac.th; piti@kmutnb.ac.th

Abstract

In this study, the influence of graphene oxide nanoparticles on the bond-slip behavior of fiber and fly ash based geopolymer paste was examined. Geopolymer paste incorporating

graphene oxide nanoparticles solution was cast in half briquetted specimens and embedded with a fiber. Three types of fibers were used: steel, polypropylene, and basalt. The pullout test was performed at two distinct speeds: 1 mm/second and 3 mm/second. Results showed that the addition of graphene oxide increased the compressive strength of geopolymer by about 7%. The bond-slip responses of fibers embedded in geopolymer mixed with graphene oxide exhibited higher peak stress and toughness as compared to those embedded in normal geopolymer. Each fiber type also showed different mode of failure. Both steel and polypropylene fibers showed full bond-slip responses due to their high ductility. Basalt fiber, on the other hand, because of its brittleness, failed by fiber fracture mode which showed no-slip in pull out responses. Both bond strength and toughness were found to be rate sensitive. The sensitivity was higher in graphene oxide/geopolymer than in conventional geopolymer.

Key words: Geopolymer; Graphene oxide; Single fiber pullout; Bond-slip; Rate sensitive.

1. Introduction

Geopolymer is another type of cementitious materials synthesized from raw materials containing high content of aluminum and silicon [1-7]. Since its chemical reaction occurs in the polymerization process, it is usually called geopolymer. The production of geopolymer requires no Portland cement and the raw materials are often byproducts or wasted materials which normally, if not being utilized, would find their ways to landfills. Therefore, the production of geopolymer is not only sustainable in term of reducing Portland cement usage, but also converting wastes from traveling to landfills.

Hardened geopolymer is known to have mechanical properties similar to that of hardened concrete produced from Portland cement. It usually exhibits excellent compressive strength but poor tensile strength. In order to improve the brittleness, short fibers are

randomly mixed with geopolymer [8-12]. The effectiveness of fiber comes from its ability to bridge across the crack to prohibit or slow down crack propagation which allows materials to carry load beyond the first cracking [13-16].

For fiber reinforced cementitious material (FRC), the performance depended on factors such as fiber type, geometry, orientation, and volume fraction [17-21]. Additionally, the mechanical properties of cementitious matrix also plays a key role in the performance of FRC, in which the improvement in mechanical properties of matrix also provides positive effect to the mechanical properties of FRC [21,22]. In practice, the properties of cementitious matrix can be enhanced using property enhancement additives. For example, phase change materials can be used to improve thermal storage [23-28], crumb rubber can be used to improve energy absorption [29-32], or nanomaterials can be used to improve mechanical properties [33-37] etc.

In this study, the effect of a nanomaterial, graphene oxide type, on the mechanical properties of fiber reinforced geopolymer (FRG) was investigated. In general, the performance of FRC can be accessed through the standard tests such as ASTM C1609 38, ASTM C1399 39 or JSCE SF4 [40] which are based mainly on flexural testing. However, in order to investigate the fiber-matrix interaction, a so-called single fiber pullout test is more appropriated [37,41,42]. The graphene oxide (GO) solution was produced at a concentration of 10 mg/ml. The incorporation rate of GO was 0.05% by weight of binder. The specimens were prepared in half-briquette form. Two loading rates of 1 and 3 mm/second were carried out. The failure pattern, bond-slip response, strength, and toughness of the obtained results were discussed.

2. Experimental process

2.1. Materials

- Binder – Class C fly ash (FA) according to ASTM C168 with a specific gravity of 2.61 and chemical composition as shown in Table 1.
- Fine aggregate – River sand (RS) with a specific gravity of 2.85 and particle size between sieve no. 4 and 16.
- Alkaline activator – Liquid solution of sodium hydroxide (SH, NaOH) and sodium silicate (SS, Na₂SiO₃) were used. The concentration of SH is set constant at 12 Molars.
- Graphene oxide (GO) – GO solution dispersed in water at a concentration of 10 mg/ml. A modified Hummers technique was used to prepare the GO. [43,44]. The properties of GO are given in Table 2.
- Fiber – Steel (SF), Polypropylene (PF), and Basalt (BF) macrofibers were used. Table 3 summarizes the properties of fibers.




Table 1 Chemical compositions of fly ash

Materials	SiO ₂	Al ₂ O ₃	Fe ₂ O ₃	CaO	MgO	Na ₂ O	K ₂ O	SO ₃	LOI
FA (%)	31.85	15.89	14.07	26.76	3.66	1.95	1.95	2.45	0.17

Table 2 Properties of graphene oxide solution

Graphene oxide solution (GO)	
Appearance	Brown/Black
Solvent	Dispersion
Concentration (mg/ml)	10

Table 3 Properties of fibers

Category	SF	PF	BF
Shape	Hooked end	Crimped	Twisted bundle
Length (mm)	35	55	43
Diameter (mm)	0.55	0.85	0.72
Tensile strength (MPa)	1345	365	900
			

2.2. Preparation of specimen

The specimens in the shape of a half briquette with the dimensions as given in Fig 1a were produced. For the control geopolymer mortar (GM), the sand to binder (s/b) ratio of 1.25, liquid to binder (l/b) ratio of 0.40 and SS/SH ratio of 1.0 were used. The mixing process began by dry mixing FA and RS for about 2 minutes. Then, SH solution was added and mixed for 1 minute. After that, SS solution was added and then mixed for another 1 minute. This similar process was also employed in preparing graphene modified geopolymer mortar (GOGM) in which the graphene oxide solution (GO) at 0.05% by weight of FA was mixed SH prior to beginning of the mixing process. The mix proportions and corresponding compressive strengths are given in Table 4.

The specimens were prepared in half briquette form using a piece of Styrofoam to block half of the briquette mold and to hold a fiber at the center as shown in Fig. 1b. Before casting, one end of the fiber was inserted through a hole at the middle of the foam to be embedded in geopolymer mortar. Another end with the length of 20 mm was exposed on the empty side. Then the mortar was poured into the mold and consolidated on a vibrating table for 10 s. The

cast specimens were covered with a plastic sheet to prevent moisture loss. After 24 hours, the specimens were demolded, wrapped in plastic sheet, and kept in a controlled temperature room at 25 °C until the date of test (28 days). Three different fibers and two different mortar types were used to produce the specimens, as listed in Table 5.

Table 4 Mix proportion and compressive strength

No.	Symbols	FA (kg/m ³)	RS (kg/m ³)	SS (kg/m ³)	SH (kg/m ³)	GO (% w/w of FA)	Compressive strength (MPa)
1	GM	879	1099	176	176	0	48.1
2	GOGM	879	1099	176	176	0.05%	50.0

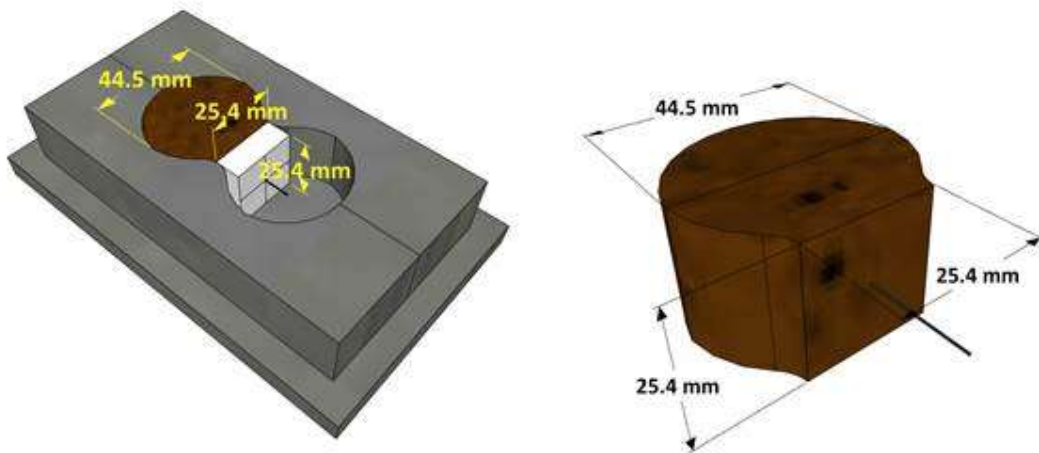


Fig. 1. Specimen preparation

Table 5 Casting schedule

Symbol	Type	Fiber	Number of sample	
			Loading rate (mm/second)	
			1	3
GM/SF	Geopolymer mortar (GM)	Steel	3	3
GM/PF		Polypropylene	3	3
GM/BF		Basalt	3	3
GOGM/SF	Geopolymer mortar with graphene oxide (GOGM)	Steel	3	3
GOGM/PF		Polypropylene	3	3
GOGM/BF		Basalt	3	3

2.3. Experimental Program

The compressive strength of geopolymer mortar (both GM and GOGM) were tested at the age of 28 days in accordance with ASTM C109 [45]. The single fiber pullout test was carried out using a 10-kN UTM machine as illustrated in Fig. 2. The effect of loading rate was examined using two different loading rates (i.e. 1 and 3 mm/second). An average of three samples was used to represent to test result.

The axial tensile stress of fiber (σ_f), average interfacial bond stress (τ_{av}), and energy absorption (E, toughness) can be calculated using Eq. (1)–(3) as follows:

$$\sigma_f = \frac{P}{A_f} \quad (1)$$

$$\tau_{av} = \frac{P}{\pi d_f L} \quad (2)$$

$$E = \int_0^{\delta} Pd\delta \quad (3)$$

Where P = pullout force (N), A_f = cross sectional area of the fiber (mm^2), L = embedded length (mm), d_f = fiber diameter (mm), and δ = fiber slipping distance (mm).



Fig. 2 The pullout test setup

3. Result and discussion

3.1. Compressive strength

The compressive strength results of the GM and GOGM at the age of 7 and 28 days are shown in Fig. 3. The 7-day strength results yielded about 70-75% of the 28-day results. The GO added at the 0.05 wt% of FA dosage insignificantly affected the 7-day compressive strength. However, it slightly increased the 28-day strength by about 8% due to the effect of

graphene oxide in promoting the geopolymerization. Similar findings were also reported, for example, Xu et al. [46] showed that GO improved the polymerization degree of fly ash geopolymer. Ranjbar et al. [47] found that addition of GO increased energy absorption during pull-out and thus led to an improvement in toughness. Saafi et al. [48] stated that rGO changed the morphology of geopolymers from a porous nature to a considerably pore filled morphology which led to an increase in compressive strength. The addition of nanoparticle like GO can reduce porosity of geopolymer with the increasing in geopolymer gel [49].

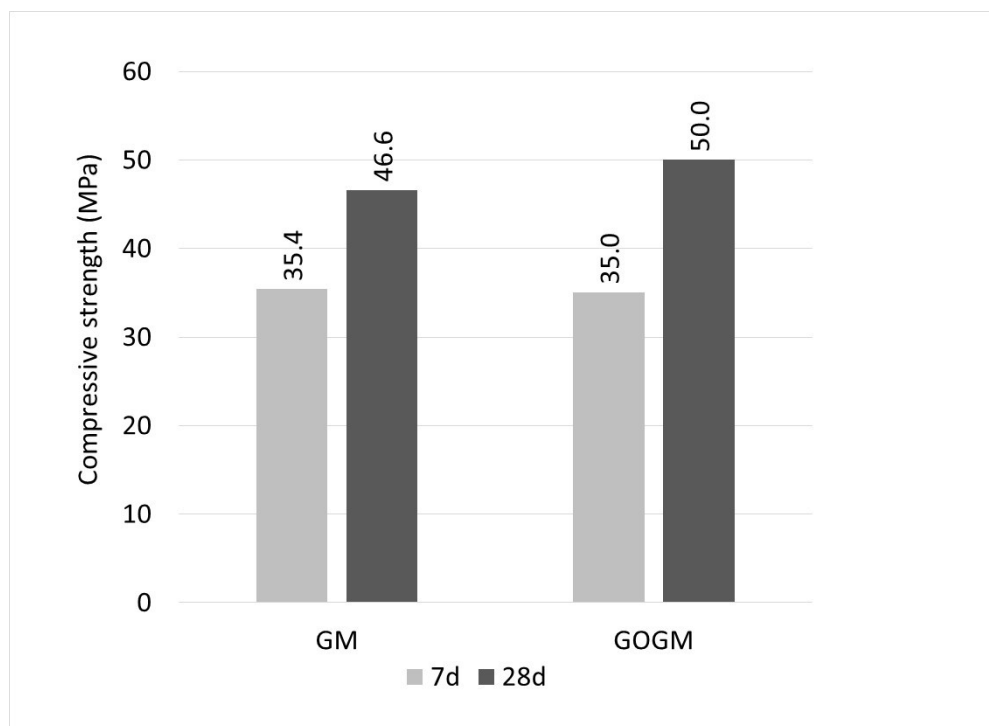


Fig.3 Compressive strength of geopolymer mortar

3.2. Energy Dispersive X-ray spectroscopy (EDS)

The EDS performed in both GM and GOGM sample are given in Table 6. The increase in carbon content (C) from 1.19 to 2.18% indicated the existence of GO in geopolymer. The geopolymerization reactions which formed N-A-S-H and Si-O-Al products were also promoted

by the addition of GO as seen by the increasing weight of Si from 13.51 to 14.72% and Na from 12.00 to 13.41% [49,50]. The addition of GO also promoted the hydration reaction which formed C-S-H product as seen by the increase in Ca content from 11.10-12.76%.

Table 6 Elemental analysis with EDS

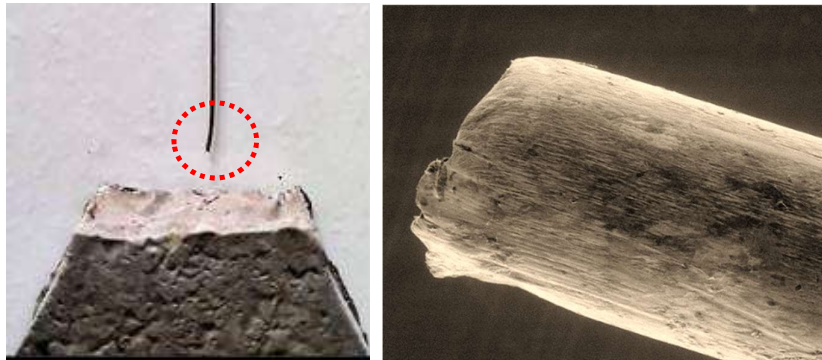
Element	Weight (%)		Atomic (%)	
	GM	GOGM	GM	GOGM
C	1.19	2.18	1.97	3.66
O	53.44	51.03	66.61	64.07
Na	12.00	13.14	10.41	11.54
Mg	1.04	1.02	0.89	0.83
Al	5.73	6.59	4.24	4.88
Si	13.51	14.72	9.60	9.41
S	2.02	1.59	1.26	1.00
Ca	11.10	12.76	5.57	6.48
Fe	3.51	3.23	1.33	1.19

3.3. Fiber pullout

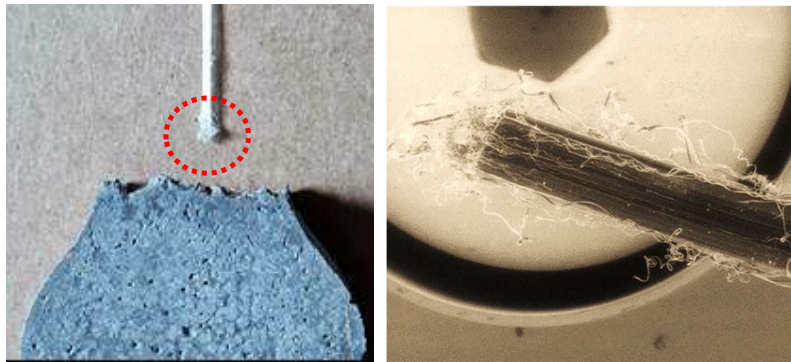
3.3.1. Failure pattern

Two types of failure patterns were observed in this study, i.e., fiber slipping and fiber fracture. The failure mode depends on fiber tensile strength and bond stress between fiber and matrix. If the fiber tensile strength is greater than the applied bond stress, the fiber slips and is completely pulled out from mortar without fiber fracture or breakage. This was found in the case of SF and PF. On the contrary to fiber slipping, when the bond strength is greater

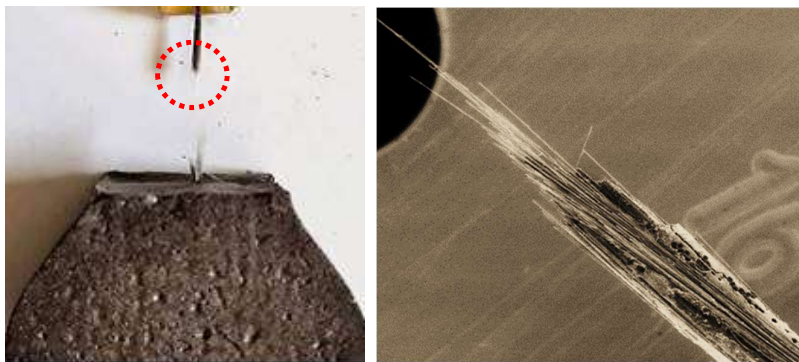
than the fiber tensile strength, fibers are broken before being completely pulled out from mortar. This failure mode is known as fiber fracture, which was observed in BF fiber.



(a)



(b)



(c)

Fig. 4 SEM images of fiber after being pulled out : (a) SF, (b) PF, and (c) BF

Fig. 4 illustrates the failure mode of each fiber type in microscopic level. For SF, the deformed part at the fiber's end (deformed end) appeared to be straightened before being pulled out entirely from mortar and no major damage to the fiber end was seen (see Fig. 4a). For PF, it appeared as though the fiber's surface was scraped against the interface between mortar and fiber during the process of pulling out seen by the occurrence of microfiber strands being scraped out along the surface. At the end of PF fiber, a severe damage was observed with large amount of fiber strands accumulating there (Fig. 4b). Noting that, although the hooked end of SF greatly increases bond strength via mechanical anchorage, its tensile strength is much greater than that. While the PF tensile strength is considerably lower than that of SF, its bonding to mortar is even lesser. Hence, both SF and PF slipped without breaking.

For BF, since BF is a twisted bundle type fiber with a coating material, partial debonding of the coating material throughout the fiber length can be noticed during the pullout (Fig. 4c). Also, for a bundle type fiber, the small spaces between each fiber strand causes the fiber to have high absorption. The high absorption allows geopolymer paste to be absorbed along the fiber surface which significantly improves the interfacial bonding between fiber and the matrix. In the case of BF, the improvement in interfacial bond was up to the point where the interfacial bond stress became higher than the fiber strength and caused fiber to fail in fracture mode (Fig 4c). At the tip of the fiber end, uneven tear and end splitting of small BF fiber strands were observed which indicated that the fiber greatly suffered large stress during the pullout process. Similar finding was reported by Chindapasirt et al [37] where glass fiber with bundle type was found to exhibit better bonding and strong interfacial bond.

3.3.2. Single fiber pullout response

Fig.6 illustrates the typical bond-slip behaviors of the single fiber pullout test schematically. The fiber pullout behavior can be categorized into pre-peak and post-peak. Initially, the entire embedded fiber is bonded or adhered to the mortar. When a fiber is subjected to a pullout load, the load is transmitted to mortar through the adhesion force. During the initial linear response, the adhesion force is developed corresponding to the applied load to keep fiber in resting condition. Once the load reaches its peak, the fiber is either fractured or begins to lose adhesion and slip.

In the case where the ultimate strength of the fiber is greater than the peak stress, the fiber is not fractured but starts to slip out of mortar (Fig. 6a). As the fiber slips, two main forces, i.e., friction force (taken place as fiber moves against mortar) and anchorage force (obtained from any mechanical anchorage and fiber geometry), govern the load carried in the post-peak response.

In the case where the ultimate strength of the fiber is lower than the peak stress, as soon as the pullout load reaches the peak, the fiber begins to fracture, and the load quickly drops to zero simultaneously (Fig. 6b).

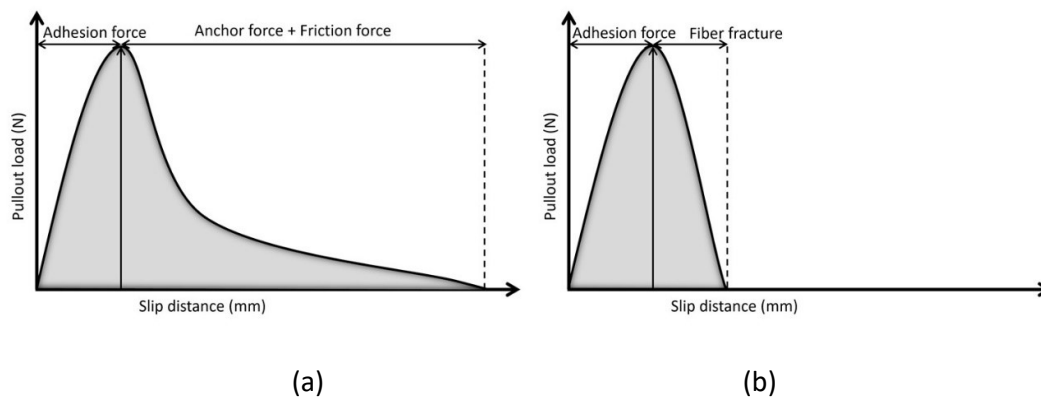


Fig.6 Typical bond-slip response of (a) Fiber pull-out and (b) Fiber fracture

(a) Effect of graphene oxide

Fig. 7a-c demonstrate the effect of graphene oxide on bond-slip response of SF, PF, and BF subjected to 1 and 3 mm/second loading rate. The bond-slip responses of SF embedded in GM and GOGM are shown in Fig. 7a. Prior to the peak, a linear bond-slip response was observed. The deformation of the steel fibers increased linearly with the increasing applied load. Once the load reached its peak, the fiber began to slip and a large drop of load occurred. Due to the smooth and hard surface of steel fiber, the interface bond was not particularly strong. However, as the fiber slipped out, the dropping of load began to slow down. The slow descending post peak response contributed mainly from the deformed shape (hooked end) at fiber end. As the fiber began to be pulling out of its resting place, the hooked end provided a resistance to the pulling force. Once the hooked end shape was forced to be straightened, the fiber was pulled out easily, and the load then descended to zero. The addition of graphene oxide appeared to increase the peak pulling load. In addition to the anchorage force, the stronger geopolymer matrix also provided an additional resistance to the pullout force. The increase in peak load in the case of SF was observed around 7% and 12% for the loading rate of 1 and 3 mm/second, respectively (Table 7 and 8).

Fig. 7b shows the bond-slip behavior of PF fiber. Similar to the case with SF, the load increased linearly with the fiber deformation prior to the peak load. However, because of the highly elastic and low strength characteristic of the polypropylene fiber, larger deformations at the peak load and smaller peak loads as compared to those of SF were observed in the case of PF. Beyond peak load, a gradual decrease of pullout load was partly due to the friction bond between fiber surface and geopolymer matrix. Another part was perhaps provided by the accumulation of scraped tiny fiber strands along the surface and at the fiber end, which provided resistance to the pulling load and helped in slowing the rate of load drop.

The post peak response of PF fiber was not quite similar to the SF. There was no large drop of load occurred after the load reaching its peak. This indicated that PF did have better bonding to geopolymer paste than SF did due to its rough and wavy surface. Right after the peak load, the load gradually descends to zero. As seen in Fig.6b, SEM image of a completely pulled out PF fiber showed an evidences of scraped fiber strands being accumulated at the fiber tip. Graphene oxide seemed to have an effect on the peak pulling force of PF in the range of 11 to 14 % (Table 7 and 8).

Fig. 7c shows the bond-slip responses of BF fiber. In the case where fiber fracture occurred, the responses were short and brittle. As soon as the load reached its peak, the fiber fracture occurred and the load fell instantaneously. The effect of GO caused the peak load to increase from 13.8 to 19.7% which were the highest among the three fibers (Table 7 and 8). This is partly because of the improvement in bond strength of the BF fiber from its high absorbability.

It must be noted here, even though, the BF fiber failed in fiber fracture mode, the axial tensile stress at peak was lower than the fiber tensile strength capacity (900 MPa) (Table 6 and 7). This can be explained as follow. Since the BF fiber are twisted bundle type fiber, this means that the small fibre strands are in fact embedded in the paste with a slightly inclined angle. This inclined angle can lead to an increase in bridging force which creates higher stresses in the fiber due to both bending and axial forces [51,52]. Choi et al. [53] reported that the tensile strength of basalt fiber decreased with an increase in the inclined angle of the fiber.

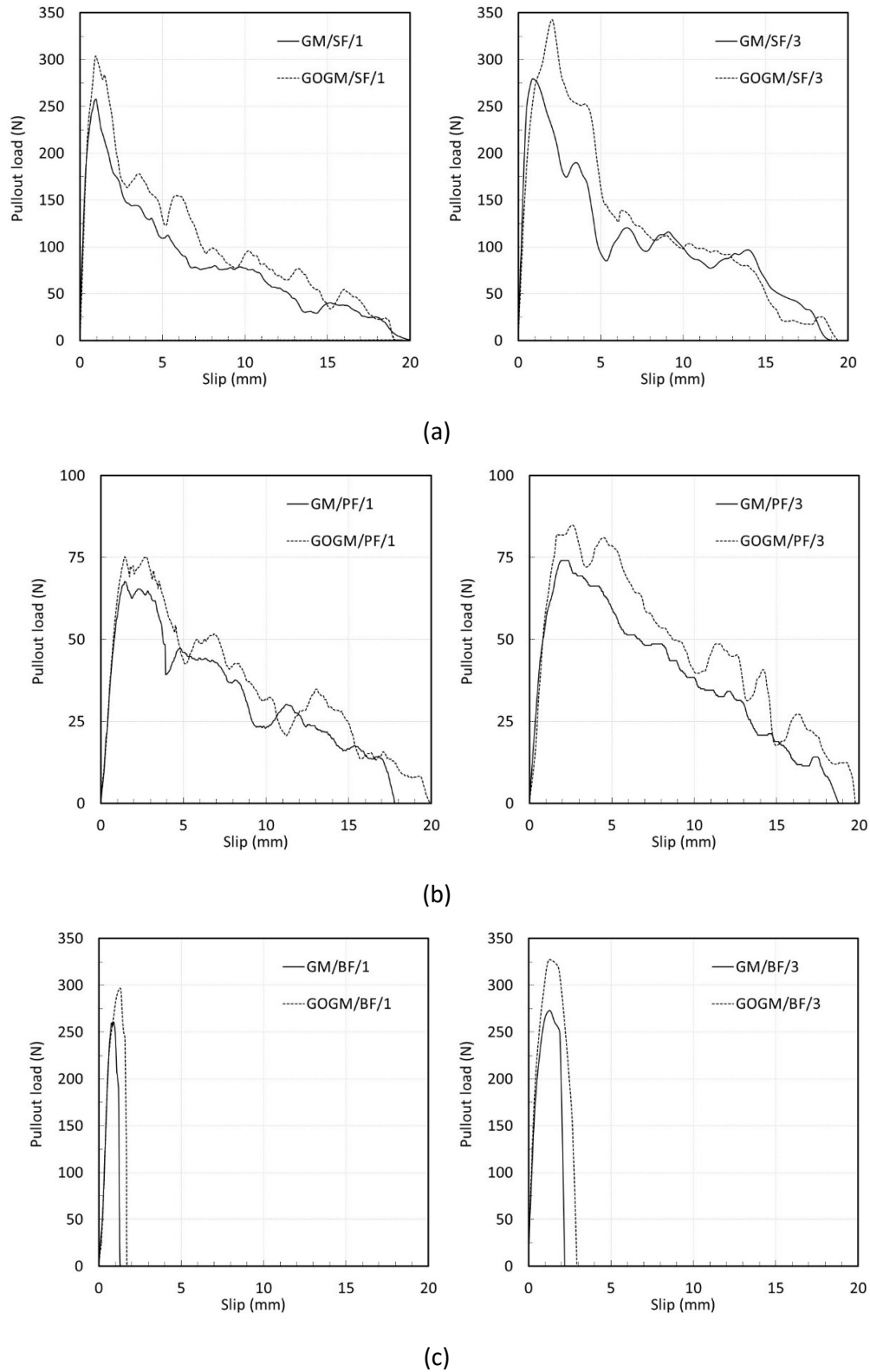


Fig. 7 Effect of graphene oxide on bond-slip responses of a) SF, b) PF, c) BF

3.3.3. Mechanical properties

Results on peak pullout load, strength, and bond strength are given in Table 6 and 7 and the pullout energy (toughness) are shown in Fig. 8. Both peak pullout stress and bond strength in GOGM (SF/GOGM, PF/GOGM, and BF/GOGM) were higher than in GM (SF/GM, PF/GM, and BF/GM). They were increased by 11-17% for the loading rate of 1 mm/sec and 14-23% for the loading rate of 3 mm/sec.

For bond-slip toughness, among the fibers, the SF provided the highest toughness (around 1620-2382 N-mm) due to its high strength and ductility. The PF, which has relatively lower strength, produced lesser toughness (around 599-914 N-mm). Even though BF has higher tensile strength than PF, their brittleness and twisted bundle alignment caused the fracture failure to occur prior to slipping. This cut short its bond-slip responses and prohibited post-peak response to occur. Thus, BF yielded the lowest toughness (around 207-682 N-mm). On the effect of GO, the toughness was found to increase at different degrees depending on the fiber type.

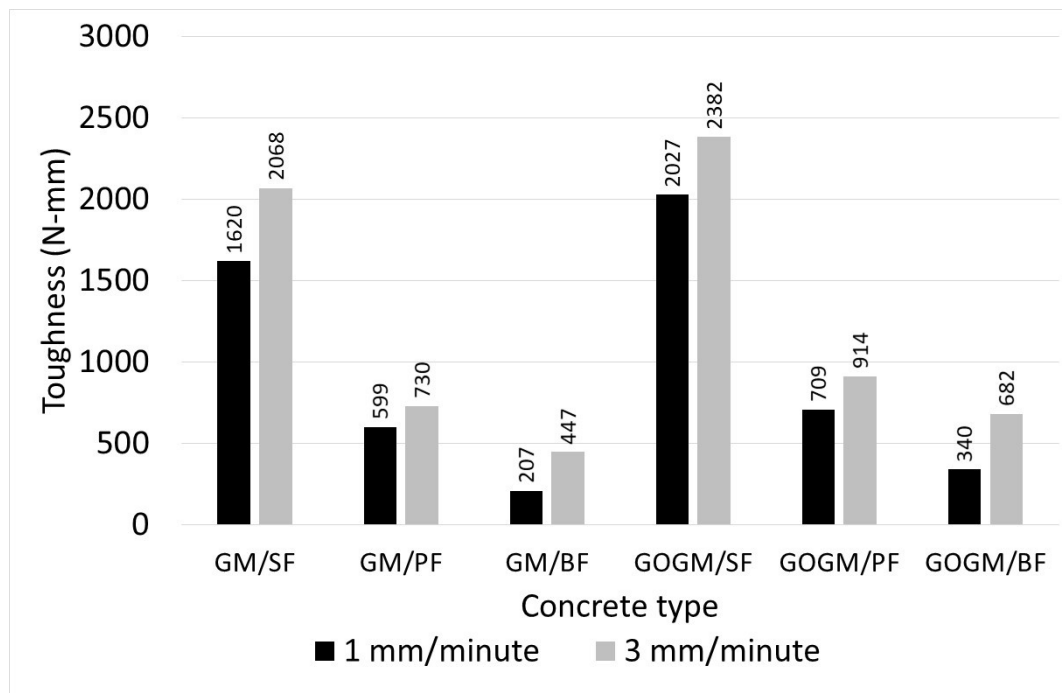
Table 7 Peak load and strength of fiber subjected 1 mm/second loading rate

Specimen type	Peak load (N)	Slip at Peak load (mm)	Tensile strength (MPa)	Avg. Bond strength (MPa)
GM/SF/1	258	1.00	1085	7.46
GM/PF/1	68	1.47	119	1.27
GM/BF/1	261	0.88	641	5.77
GOGM/SF/1	303	0.94	1276	8.77
GOGM/PF/1	75	1.46	132	1.41

GOGM/BF/1	297	1.30	729	6.56
-----------	-----	------	-----	------

Table 8 Peak load and stress of fiber subjected 3 mm/second loading rate

Specimen type	Peak load (N)	Slip at Peak load (mm)	Tensile strength (MPa)	Avg. Bond strength (MPa)
GM/SF/3	278	0.83	1171	8.05
GM/PF/3	74	1.92	131	1.39
GM/BF/3	273	1.28	671	6.04
GOGM/SF/3	342	2.06	1441	9.91
GOGM/PF/3	85	2.55	149	1.59
GOGM/BF/3	327	1.23	803	7.23

**Fig. 8** Pullout energy or Toughness

Comparing between GM and GOGM, the different percentage in peak load at two different rates of loading is shown in Fig. 9. For GM, the increase in peak load was found at around 8, 9.6, and 4.8% for GM/SF, GM/PF, and GM/BF, respectively. For GOGM, the increase in peak load was observed around 12.9, 12.9, and 11.2% for GOGM/SF, GOGM/PF, and GOGM/BF, respectively. This indicated that the GOGM is more sensitive to the rate of loading than GO. This perhaps has to do with the increase matrix strength which provides more resistance to the pull force.

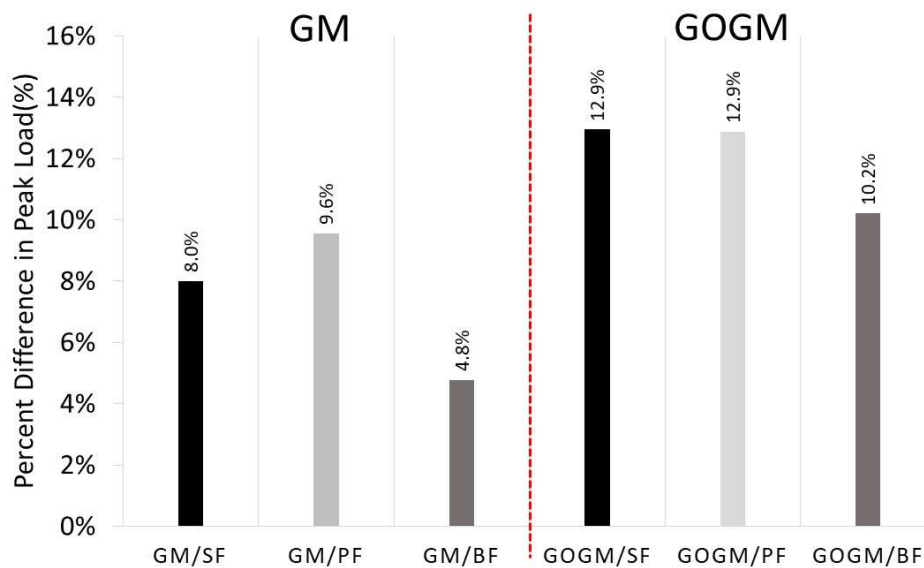


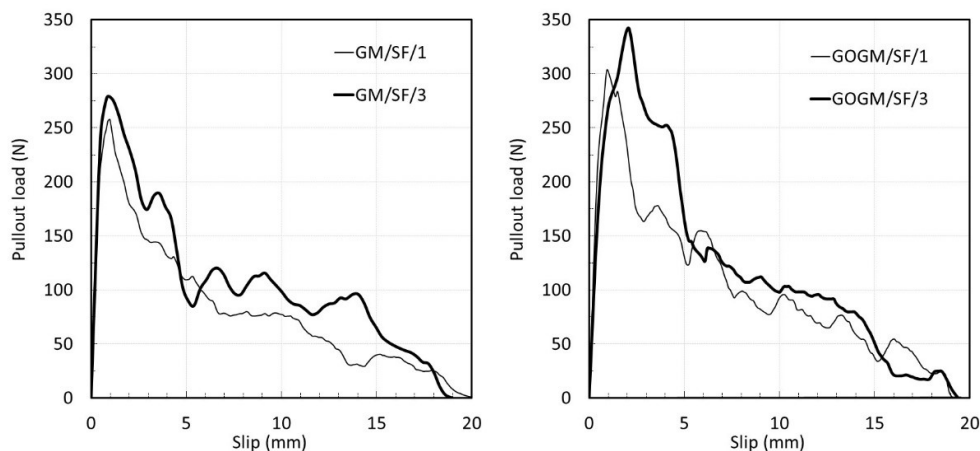
Fig. 9 Percent difference in peak load due to increasing loading rate comparing between GM and GOGM

(b) Effect of loading rate on bond-slip response

Fig. 10a-c shows the effect of loading rate on the bond-slip responses. Regardless of fiber and mortar type, the increase loading rate caused the peak load to increase. Results given in Table 7 and 8, indicated the increase of about 8.0, 9.6, and 4.8% in GM/SF, GM/PF, GM/BF, respectively.

and GM/BF, respectively. Theoretically, the mechanical properties of composite materials like fiber reinforced cementitious materials are known to be sensitive to the loading rate, meaning that they increase as the rate of loading increases [54-61]. This is also the case for the single pull-out test. Babafemi [62] reported the increase in pullout load of macro synthetic fiber with the increasing rate of loading and embedment length. Bindiganavile [63] found the increase in peak pullout load and the change in mode of failure as the load scheme changed from quasi-static to impact pull out load. Comparing among three fibers, the BF fiber is less sensitive than both SF and PF. This is perhaps due to the failure of BF fiber which failed by fracture mode.

In the case of GOGM, the increase of about 12.7, 12.9, and 10.2% were observed for GOGM/SF, GOGM/PF, and GOGM/BF, respectively. The GOGM appears to be more sensitive to loading rate than GM as seen by the higher increasing percentage. This contributes mainly to the higher compressive strength of GOGM due to addition of graphene oxide. Kim et al similarly reported the increase in rate sensitivity of fiber embedded in cement material with higher compressive strength [64].



(a)

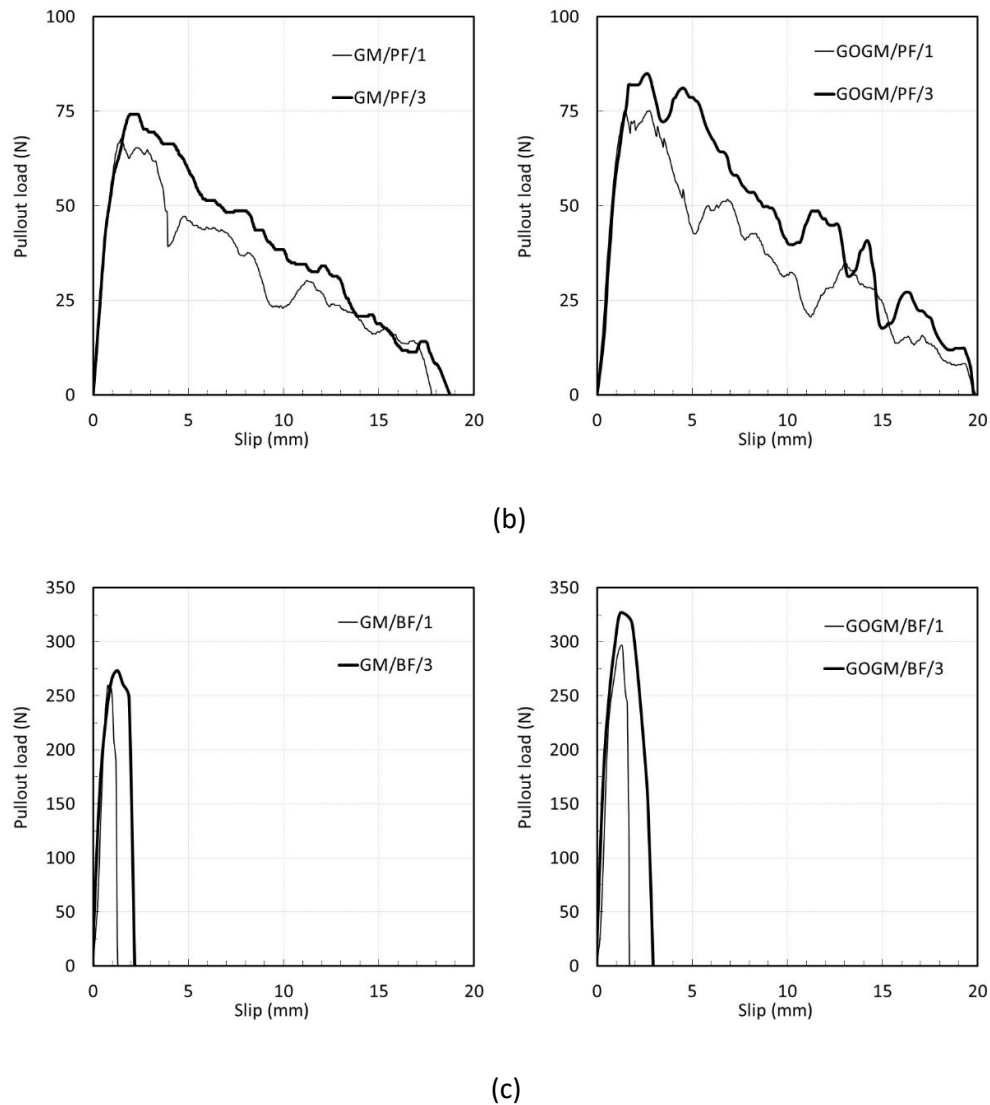


Fig. 10 Effect of loading rate on bond-slip responses of a) SF, b) PF, c) BF

4. Conclusions

The addition of graphene oxide at the dosage of 0.05% weight of binder (fly ash) increased the compressive strength of GM by about 7.3%.

From the single fiber pullout test, the failure mode of SF and PF fiber was in fiber slipping mode while BF fiber was in fiber fracture mode. The SEM revealed that the surface of PF was being scraped against the matrix which caused the accumulation of tiny fiber strands at the

end of fiber tip. For BF, the fracture of individual fiber was observed, there were signs of fiber being tortured and fractured unevenly.

For the pullout response, because of their high ductility, both SF and PF showed full bond-slip responses. The effect of GO increased both bond strength and toughness of both fibers, though at different degrees depending on fiber type. For BF fiber, the response was brittle and there was no fiber slip part because the fibre fractured before being slip out from the matrix. The effect of GO also yielded higher peak bond stress and toughness.

For the effect of loading rate, both bond strength and toughness were found to be dependent on the loading rate. With the increase loading rate from 1 to 3 mm/second, the peak bond stress increased by about 5-10% for GM and 10-12% for GOGM mortar and the toughness increased by 6-116% for GM and 19-46% for GOGM mortar.

Acknowledgement

The research is funded by National Research Council of Thailand (NRCT), and the National Science, Research and Innovation Fund (NSRF) and King Mongkut's University of Technology North Bangkok (KMUTNB) under the contract no. KMUTNB-FF-66-02. The authors would like to acknowledge PhD scholarship from King Mongkut's University of Technology North Bangkok (KMUTNB) under the contract no. KMUTNB-PHD-62-06 and Thailand Research Fund under the contract no. RTA6280012.

References

- 1 Duxson, P., Fernández-Jiménez, A., Provis, J.L. et al. (2007). Geopolymer technology: the current state of the art. *Journal of Materials Science*, 42, 2917–2933, <https://doi.org/10.1007/s10853-006-0637-z>

- 2 Sukontasukkul, P, Chindaprasirt, P, Pongsopha, P, Phoo-Ngernkham, T, Tangchirapat, W, Banthia, N. (2020). Effect of fly ash/silica fume ratio and curing condition on mechanical properties of fiber-reinforced geopolymer. *Journal of Sustainable Cement Based Materials*, 9(4):218-232.
- 3 Wang H., Li H., Yan F., (2005). Synthesis and mechanical properties of metakaolinite-based geopolymer, *Colloids and Surfaces A: Physicochemical and Engineering Aspects*, 268 (1-3), 1-6, <https://doi.org/10.1016/j.colsurfa.2005.01.016>.
- 4 Wongsas, A., Siri wattanakarn, A., Nuaklong, P., Sata, V., Sukontasukkul, P., & Chindaprasirt, P. (2020). Use of recycled aggregates in pressed fly ash geopolymer concrete. *Environmental Progress and Sustainable Energy*, 39(2) doi:10.1002/ep.13327
- 5 Lloyd, N. and Rangan, B., (2010). Geopolymer Concrete with Fly Ash, in Zachar, J. and Claisse, P. and Naik, T. and Ganjian, G. (ed), *Second International Conference on Sustainable Construction Materials and Technologies*, 3, 1493-1504. Ancona, Italy.
- 6 Suksiripattanapong, C., Krosoongnern, K., Thumrongvut, J., Sukontasukkul, P., Horpibulsuk, S., & Chindaprasirt, P. (2020). Properties of cellular lightweight high calcium bottom ash-portland cement geopolymer mortar. *Case Studies in Construction Materials*, 12 doi:10.1016/j.cscm.2020.e00337
- 7 Hanjitsuwan, S., Injorhor, B., Phoo-ngernkham, T., Damrongwiriyanupap, N., Li, L. -, Sukontasukkul, P., & Chindaprasirt, P. (2020). Drying shrinkage, strength and microstructure of alkali-activated high-calcium fly ash using FGD-gypsum and dolomite as expansive additive. *Cement and Concrete Composites*, 114 doi:10.1016/j.cemconcomp.2020.103760

- 8 Midhun, M.S., Rao, T.D.G., Srikrishna, T.C., (2018). Mechanical and fracture properties of glass fiber reinforced geopolymer concrete, *Advances in Concrete Construction*, 6(1), 29-45. DOI: <http://dx.doi.org/10.12989/acc.2018.6.1.029>
- 9 Sukontasukkul, P., Pongsopha, P., Chindaprasirt, P., & Songpiriyakij, S. (2018). Flexural performance and toughness of hybrid steel and polypropylene fibre reinforced geopolymer. *Construction and Building Materials*, 161, 37-44. doi:10.1016/j.conbuildmat.2017.11.122
- 10 Noushini, A., Hastings, M., Castel, A., Aslani, F., (2018). Mechanical and flexural performance of synthetic fibre reinforced geopolymer concrete, *Construction and Building Materials*, 186, 454-475, <https://doi.org/10.1016/j.conbuildmat.2018.07.110>.
- 11 Nuaklong, P., Wongsas, A., Boonserm, K., Ngohpok, C., Jongvivatsakul, P., Sata, V., Chindaprasirt, P. (2021). Enhancement of mechanical properties of fly ash geopolymer containing fine recycled concrete aggregate with micro carbon fiber. *Journal of Building Engineering*, 41 doi:10.1016/j.jobbe.2021.102403
- 12 Wongruk, R., Songpiriyakij, S., Sukontasukkul, P., & Chindaprasirt, P. (2015). Properties of steel fiber reinforced geopolymer doi:10.4028/www.scientific.net/KEM.659.143
- 13 Wongprachum, W., Sappakittipakorn, M., Sukontasukkul, P., Chindaprasirt, P., & Banthia, N. (2018). Resistance to sulfate attack and underwater abrasion of fiber reinforced cement mortar. *Construction and Building Materials*, 189, 686-694. doi:10.1016/j.conbuildmat.2018.09.043
- 14 Sukontasukkul, P. (2004). Tensile behaviour of hybrid fibre-reinforced concrete. *Advances in Cement Research*, 16(3), 115-122. doi:10.1680/adcr.16.31.115.41516

- 15 Sukontasukkul, P., & Mindess, S. (2003). The shear fracture of concrete under impact loading using end confined beams. *Materials and Structures/Materiaux Et Constructions*, 36(6), 372-378. doi:10.1007/bf02481062
- 16 Sukontasukkul, P., Chaisakulkiet, U., Jamsawang, P., Horpibulsuk, S., Jaturapitakkul, C., & Chindaprasirt, P. (2019). Case investigation on application of steel fibers in roller compacted concrete pavement in thailand. *Case Studies in Construction Materials*, 11 doi:10.1016/j.cscm.2019.e00271
- 17 Soroushian P. and Bayasi Z., (1991). Fiber Type Effects on the Performance of Steel Fiber Reinforced Concrete, *Materials Journal*, 88(2), 129-134
- 18 Yao W., Li J., Wu K., (2003). Mechanical properties of hybrid fiber-reinforced concrete at low fiber volume fraction, *Cement and Concrete Research*, 33(1), 27-30, [https://doi.org/10.1016/S0008-8846\(02\)00913-4](https://doi.org/10.1016/S0008-8846(02)00913-4).
- 19 Sukontasukkul, P., Jamnam, S., Sappakittipakorn, M., Fujikake, K., & Chindaprasirt, P. (2018). Residual flexural behavior of fiber reinforced concrete after heating. *Materials and Structures/Materiaux Et Constructions*, 51(4) doi:10.1617/s11527-018-1210-3
- 20 Soroushian P., Lee C.D., (1990). Distribution and Orientation of Fibers in Steel Fiber Reinforced Concrete, *Materials Journal*, 87(5), 433-439
- 21 Lee J.H., Cho B.S., Choi E.S., (2017). Flexural capacity of fiber reinforced concrete with a consideration of concrete strength and fiber content, *Construction and Building Materials*, 138, 222-231, <https://doi.org/10.1016/j.conbuildmat.2017.01.096>.
- 22 Song P.S., Hwang S.(2004). Mechanical properties of high-strength steel fiber-reinforced concrete, *Construction and Building Materials*, 18(9), 669-673, <https://doi.org/10.1016/j.conbuildmat.2004.04.027>.

- 23 Sukontasukkul, P., Nontiyutsirikul, N., Songpiriyakij, S., Sakai, K., & Chindapasirt, P. (2016). Use of phase change material to improve thermal properties of lightweight geopolymer panel. *Materials and Structures/Materiaux Et Constructions*, 49(11), 4637-4645. doi:10.1617/s11527-016-0812-x
- 24 Sukontasukkul, P., Sutthiphasilp, T., Chalodhorn, W., & Chindapasirt, P. (2019). Improving thermal properties of exterior plastering mortars with phase change materials with different melting temperatures: Paraffin and polyethylene glycol. *Advances in Building Energy Research*, 13(2), 220-240. doi:10.1080/17512549.2018.1488614
- 25 Sukontasukkul, P., Intawong, E., Preemanoch, P., & Chindapasirt, P. (2016). Use of paraffin impregnated lightweight aggregates to improve thermal properties of concrete panels. *Materials and Structures/Materiaux Et Constructions*, 49(5), 1793-1803. doi:10.1617/s11527-015-0612-8
- 26 Sukontasukkul, P., Uthaichotirat, P., Sangpet, T., Sisomphon, K., Newlands, M., Siripanichgorn, A., & Chindapasirt, P. (2019). Thermal properties of lightweight concrete incorporating high contents of phase change materials. *Construction and Building Materials*, 207, 431-439. doi:10.1016/j.conbuildmat.2019.02.152
- 27 Uthaichotirat, P., Sukontasukkul, P., Jitsangiam, P., Suksiripattanapong, C., Sata, V., & Chindapasirt, P. (2020). Thermal and sound properties of concrete mixed with high porous aggregates from manufacturing waste impregnated with phase change material. *Journal of Building Engineering*, 29 doi:10.1016/j.job.2019.101111
- 28 Sukontasukkul, P., Sangpet, T., Newlands, M., Yoo, D. -, Tangchirapat, W., Limkatanyu, S., & Chindapasirt, P. (2020). Thermal storage properties of lightweight concrete incorporating phase change materials with different fusion points in hybrid form for high temperature applications. *Heliyon*, 6(9) doi:10.1016/j.heliyon.2020.e04863

- 29 Chaikaew, C., Sukontasukkul, P., Chaisakulkiet, U., Sata, V., & Chindaprasirt, P. (2019). Properties of concrete pedestrian blocks containing crumb rubber from recycle waste tyres reinforced with steel fibres. *Case Studies in Construction Materials*, 11 doi:10.1016/j.cscm.2019.e00304
- 30 Hasanzadeh, M., Rezaifar, O., Gholhaki, M., & Kazem Sharbatdar, M. (2021). Performance optimization of ground rubberized green concrete with metakaolin. *Structures*, 34, 433-448. doi:10.1016/j.istruc.2021.08.006
- 31 Maho, B., Sukontasukkul, P., Jamnam, S., Yamaguchi, E., Fujikake, K., & Banthia, N. (2019). Effect of rubber insertion on impact behavior of multilayer steel fiber reinforced concrete bulletproof panel. *Construction and Building Materials*, 216, 476-484. doi:10.1016/j.conbuildmat.2019.04.243
- 32 Pongsopha, P., Sukontasukkul, P., Maho, B., Intarabut, D., Phoo-ngernkham, T., Hanjitsuwan, S., Limkatanyu, S. (2021). Sustainable rubberized concrete mixed with surface treated PCM lightweight aggregates subjected to high temperature cycle. *Construction and Building Materials*, 303 doi:10.1016/j.conbuildmat.2021.124535
- 33 Said, A. M., Zeidan, M. S., Bassuoni, M. T., & Tian, Y. (2012). Properties of concrete incorporating nano-silica. *Construction and Building Materials*, 36, 838-844. doi:10.1016/j.conbuildmat.2012.06.044
- 34 Nuaklong, P., Boonchoo, N., Jongvivatsakul, P., Charinpanitkul, T., & Sukontasukkul, P. (2021). Hybrid effect of carbon nanotubes and polypropylene fibers on mechanical properties and fire resistance of cement mortar. *Construction and Building Materials*, 275 doi:10.1016/j.conbuildmat.2020.122189

- 35 Tontiwattanukul, K., Sanguansin, J., Ratanavaraha, V., Sata, V., Limkatanyu, S., & Sukontasukkul, P. (2021). Effect of viscoelastic polymer on damping properties of precast concrete panel. *Heliyon*, 7(5) doi:10.1016/j.heliyon.2021.e06967
- 36 Li, W., Huang, Z., Cao, F., Sun, Z., & Shah, S. P. (2015). Effects of nano-silica and nano-limestone on flowability and mechanical properties of ultra-high-performance concrete matrix. *Construction and Building Materials*, 95, 366-374. doi:10.1016/j.conbuildmat.2015.05.137
- 37 Chindaprasirt, P., Sukontasukkul, P., Techaphatthanakon, A., Kongtun, S., Ruttanapun, C., Yoo, D. -, Banthia, N. (2021). Effect of graphene oxide on single fiber pullout behavior. *Construction and Building Materials*, 280 doi:10.1016/j.conbuildmat.2021.122539
- 38 ASTM C1609 / C1609M-19a, Standard Test Method for Flexural Performance of Fiber-Reinforced Concrete (Using Beam With Third-Point Loading), ASTM International, West Conshohocken, PA, 2019, www.astm.org
- 39 ASTM C1399 / C1399M-10(2015), Standard Test Method for Obtaining Average Residual-Strength of Fiber-Reinforced Concrete, ASTM International, West Conshohocken, PA, 2015, www.astm.org
- 40 JSCE AF4, Method of Test For Flexural Strength and Flexural Toughness, JSCE, Japan, 1984.
- 41 Yoo, D.Y., Park, J.J., Kim, S.W., (2017). Fiber pullout behavior of HPRCC: Effects of matrix strength and fiber type, *Composite Structures*, 174, 263-276, <https://doi.org/10.1016/j.compstruct.2017.04.064>.
- 42 Yoo, D.Y., Je, J.H., Choi, H.J., Sukontasukkul, P., (2020). Influence of embedment length on the pullout behavior of steel fibers from ultra-high-performance concrete, *Materials Letters*, 276, <https://doi.org/10.1016/j.matlet.2020.128233>.
- 43 C. Phrompet, C. Sriwong, P. Srepusharawoot, S. Maensiri, P. Chindaprasirt, and C.

- Ruttanapun, "Effect of free oxygen radical anions and free electrons in a Ca₁₂Al₁₄O₃₃ cement structure on its optical, electronic and antibacterial properties," *Heliyon*, vol. 5 (5), e01808, 2019.
- 44 C. Phrompet, C. Sriwong, and C. Ruttanapun, "Mechanical, dielectric, thermal and antibacterial properties of reduced graphene oxide (rGO)-nanosized C₃AH₆ cement nanocomposites for smart cement-based materials," *Compos. Part B Eng.*, 175, 2019.
- 45 ASTM C109/C109M, 2013, Standard Test Method for Compressive Strength of Hydraulic Cement Mortars (Using 2-in. or [50-mm] Cube Specimens). ASTM International, West Conshohocken, PA.
- 46 G. Xu, J. Zhong, and X. Shi, "Influence of graphene oxide in a chemically activated fly ash," *Fuel*, 226, 644–657, 2018.
- 47 N. Ranjbar, M. Mehrali, M. Mehrali, UJ. Alengaram, and MZ. Jumaat. "Graphene nanoplatelet-fly ash based geopolymer composites." *Cem Concr Res*; 76, 222–31, 2015.
- 48 M. Saafi, L. Tang, J. Fung, M. Rahman, and J. Liggat, "Enhanced properties of graphene/fly ash geopolymeric composite cement," *Cem. Concr. Res.*, 67, 292–299, 2015.
- 49 X. Liu *et al.*, "Effects of graphene oxide on microstructure and mechanical properties of graphene oxide-geopolymer composites," *Constr. Build. Mater.*, 247, 118544, 2020.
- 50 P. Jittabut, S. Horpibulsuk, Physical and microstructure properties of geopolymer nanocomposite reinforced with carbon nanotubes, *materialstoday: PROCEEDINGS*, 17 (2019), 1682-1692, <https://doi.org/10.1016/j.matpr.2019.06.199>.
- 51 A. Katz and V. C. Li, "Inclination Angle Effect of Carbon Fibers in," *J. Eng. Mech.*, 121, 1340–1348, 1995.
- 52 J. Zhang and V. C. Li, "Effect of inclination angle on fiber rupture load in fiber reinforced cementitious composites," *Compos. Sci. Technol.*, 62(6), 775–781, 2002.

- 53 J. Choi and B. Y. Lee, "Bonding Properties of Basalt Fiber and Strength Reduction According to Fiber Orientation," *Materials*, 8, 6719–6727, 2015,
- 54 Bentur, A., Mindess, S. & Banthia, N. The behaviour of concrete under impact loading: Experimental procedures and method of analysis. *Materials and Structures* 19, 371–378, 1986.
- 55 P. Sukontasukkul, P. Nimityongskul, S. Mindess, Effect of loading rate on damage of concrete, *Cement and Concrete Research*, 34(11), 2127-2134, 2004
- 56 V. Bindiganavile and N. Banthia, Polymer and Steel Fiber-Reinforced Cementitious Composites under Impact Loading—Part 2: Flexural Toughness, *Materials Journal*, 98(1), 17-24, 2001.
- 57 P. Sukontasukkul, S. Mindess, N. Banthia Properties of confined fibre-reinforced concrete under uniaxial compressive impact, *Cement and concrete research*, 35(1), 11-18, 2005.
- 58 P. Sukontasukkul, S. Mindess, The shear fracture of concrete under impact loading using end confined beams, *Materials and Structures*, 36(6), 372-378, 2003
- 59 P. Sukontasukkul, F. Lam, S. Mindess, Fracture of parallel strand lumber (PSL) under impact loading, *Materials and Structures* 33 (7), 445-449, 2005.
- 60 B. Maho, P. Sukontasukkul, S. Jamnam, E. Yamaguchi, K Fujikake, N. Banthia, Effect of rubber insertion on impact behavior of multilayer steel fiber reinforced concrete bulletproof panel, *Construction and Building Materials*, 216, 476-484, 2019
- 61 P. Sukontasukkul, S. Mindess, N. Banthia, T. Mikami, Impact resistance of laterally confined fibre reinforced concrete plates, *Materials and Structures* 34 (10), 612-618, 2001.
- 62 A.J. Babafemi, W.P. Boshoff, Pull-out response of macro synthetic fibre from concrete matrix: Effect of loading rate and embedment length, *Construction and Building Materials*,

135, 2017, 590-599

- 63 V. Bindiganavile and N. Banthia, Polymer and Steel Fiber-Reinforced Cementitious Composites under Impact Loading —Part 1: Bond-Slip Response, *Materials Journal*, 98(1), 10-16, 2001.
- 64 D.J. Kim, S. El-Tawil, Sherif, A.E., Naaman, Loading Rate Effect on Pullout Behavior of Deformed Steel Fibers, *ACI Materials Journal*, 105(6), 576-584, 2008